Experimental comparison of the flow-induced loading between a ducted bottom-mounted twin vertical axis tidal turbine at still and an unducted prototype

Y. Saouli, R. Coquet, JV. Facq, B. Gaurier, G. Germain, B. Gomez, N. Marcon, G. Maurice, M. Moreau.

***Abstract*—The FloWatt project is dedicated to actively participate to renewable energy exploitation by developing an innovative design of tidal turbine for high energetic sites as the Raz-Blanchard, France. Works related to the HydroQuest's 1 MW-rated demonstrator deployment on the site of Paimpol-Brehat allowed to successfully initiate the new generation development, presenting better optimization and performance. Along these past three years, studies at 1/20 scale have been conducted in the wave and current circulating tank of Ifremer to compare the results obtained at both scales for the first generation of machines. Tests have been carried out for the new generation at 1/20 scale to validate the new design. Various points of comparison will thus be discussed in this paper. The first part of the paper presents the FloWatt project, the means useful to the test campaigns and the models designs for both generations of turbines. Thereafter, the overall loads and moments applied to the prototypes according to the models configuration (turbine/base) are compared. Lower loadings are highlighted in the case of the new generation of machines based on proper reference areas. Machines behaviour related to the angle of incidence of the flow is also discussed, and an analyse of waves and current interaction effects on loads and moments applied to the new design is made for various wave cases.**

***Index Terms*—FloWatt, Tidal energy, Vertical axis turbine, Flume tank.**

I. Overview of the project progress

A. Presentation of the FloWatt project

IN a context where environmental issues are a major concern, renewable energy technologies show an important growth. Among them, tidal energy converters are shown to be encouraging as very energetic sites are spotted and investigated in various regions, mainly located in France and in the United Kingdom [1]. Thanks to the emerging projects, the tidal energy field is becoming competitive. Developed in the Alderney Race site, one of the most energetic marine sites on the planet, the FloWatt project aims to prove the efficiency of the HydroQuest's 2.5 MW turbine for a commercial farm deployment in the English Channel planned by 2030. Seven 2.5 MW-rated vertical axis turbines will be manufactured by CMN in Cherbourg and installed on site as illustrated on Fig. 1. The scientific research project makes possible the industrial developments led by Qair, HydroQuest and CMN. Indeed, high potential tidal turbine sites present complex characteristics, an in-depth study is necessary in order to lead to a real technological breakthrough. A first marine demonstrator with a unit power of 1 MW has been tested during two years on the test site of Paimpol Brehat, from 2019 to 2021. Fig. 2 shows the immersion process of the 1 MW-rated turbine. Its successful deployment has allowed the validation of the preliminary developments of the 2.5 MW vertical axis turbine design. These studies are based on previous farm data measurements as in [2], numerical simulations [3] - [4] and experimental simulations [5] - [6].

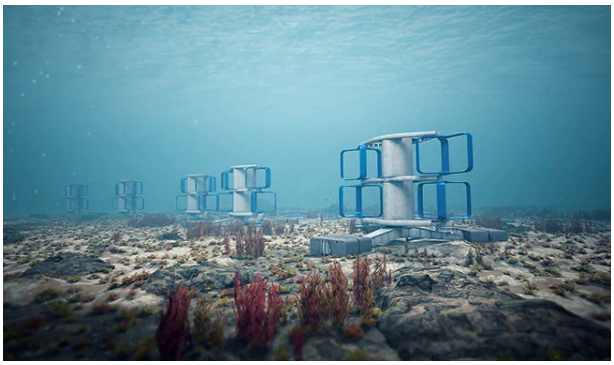

Fig. 1. Artist's rendering of the pilot farm FloWatt project based on the new generation of turbines.

Numerical models are used in order to evaluate the tidal potential of the sites, while 3D models like Telemac3D operate to determine the efficiency of tidal turbines under various flow conditions. To complete numerical data, in-situ measurements are carried out to deepen the knowledge of the site conditions. To do so, high technology tools are used to finely characterize the quantities on site, as High Frequency and X-Band radars. Experimental work is carried out in the Ifremer wave and current flume tank, at a 1/20 scale, to

Y. Saouli and M.Moreau are with HydroQuest SAS and the French Research Institute for the Exploitation of the Sea (IFREMER) Centre Manche Mer du Nord, Boulogne-sur-Mer FR-62321, France. (e-mail: yanis.saouli@ifremer.fr)

G. Germain, B. Gaurier, JV. Facq and B. Gomez are with the French Research Institute for the Exploitation of the Sea (IFREMER) Centre Manche Mer du Nord, Boulogne-sur-Mer FR-62321, France. (e-mail: gregory.germain@ifremer.fr).

G. Maurice, N. Marcon and R. Coquet are with HydroQuest SAS, 16 Chemin de Malacher, Meylan FR-38240, France. (e-mail: guillaume.maurice@hydroquest.net).

Digital Object Identifier:https://doi.org/10.36688/ewtec-2023-498

characterize the behaviour of the machine in various operating situations. All these development steps are helpful in the comprehension of the machine response to environmental constraints and lead to design optimization. One of the main turning points will be the deployment of a first demonstrator of the new generation in the coming years.

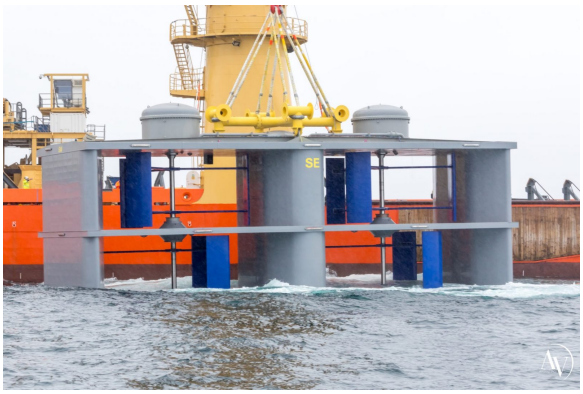

Fig. 2. HydroQuest demonstrator immersion at Paimpol-Brehat test site in April 2019.

For the first generation of machines, data collected in-situ have been compared to the results obtained from numerical models and experimental tests, validating the industrial tools to ensure the growth of this industry. As a part of the development of the future machines, it is essential to validate the new design through a test campaign. The experimental work will emphasize the design-induced variations, allowing a better comprehension of the machine operation for various flow conditions, with possible analogies appearing between both 1/20 models generations.
In this paper, we will compare at 1/20 scale the loads and moments applied to both machines (1 MW-rated and 2.5 MW-rated machines). Both test campaigns have been made in the same basin, with similar experimental conditions. Loads due to current only will first be evaluated, then the impact of waves-current interaction will be studied. Main differences between both designs will thus be highlighted.

II. Experimental set-up

Test campaigns are carried out in the wave and current circulating tank of Ifremer in Boulogne-sur-Mer at 1/20 scale in order to characterize the machine behaviour under flow conditions chosen as close to those found at sea. To do so, the comparison will be based on the study of coefficients depending on the loads/moments measurements and the geometry of each model. The drag and tilting moment coefficients, respectively noted C_x and C_{My}, are defined as follows :

$$C_x(t) = \frac{F_x(t)}{\frac{1}{2}\rho S U_{ref}^2} \quad (1)$$

$$C_{My}(t) = \frac{M_y(t)}{\frac{1}{2}\rho S L U_{ref}^2} \quad (2)$$

with ρ the volumetric mass density, S the reference area, U_{ref} the current velocity upstream and L the reference length of the models. F_x is the load applied in the flow direction, and M_y is the tilting moment of the model. The reference area of each machine will be presented in the following subparts.

The designs of the two models are first introduced, then the experimental setup and the flow characteristics are then presented.

A. Ducted prototype characteristics (Gen1)

The ducted prototype here (Fig. 3) is the 1/20 model geometrically similar to the 1 MW-rated demonstrator that has been deployed in situ during two years at the Paimpol Brehat site. It will be defined in the following as Gen1. The model is composed of two counter-rotating vertical axis rotor columns, each one made of two levels of rotors with a 60° phase difference between them. At that scale, the total model height is h_{m1} = 0.840 m and its width is W_{m1} = 1.240 m. The distance from the bottom to the top horizontal plates defines the turbine height (equal to H_{m1} = 0.450 m). The rotors are : h_{r1} = 0.190m and R_{m1} = 0.200 m respectively for the height and the radius, with blades chord of 73 mm. The turbine is fixed on a tripod base to model the real demonstrator gravity base. A six-component load cell with a range of 150 daN is placed at the interface turbine/base in order to measure the loads applied to the turbine only. Another load cell is placed below the whole structure to measure the overall loads applied to the turbine and the base, with a capacity of 2000 daN.

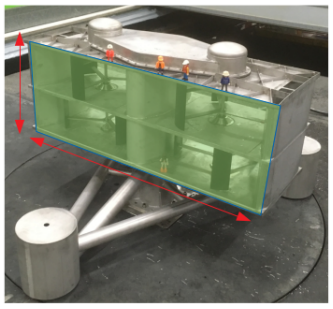

Fig. 3. Picture of the Gen1 model. The green area (defined as the model capture area) and the front surface of the base represent the total area used to normalize the hydrodynamic coefficients.

More details about this prototype are given in [2].The test campaigns have been conducted in order to characterize performance for various flow conditions in terms of angle of incidence, vertical velocity profile, turbulence and waves.

The surface area of interest here is the capture area $H_{m1} \times W_{m1}$ added to the front surface of the base to the flow (green zone in Fig.3 composed the reference area when we study the turbine only). The distance between each rotor columns is also taken as a reference length, with L_1 = 0.63 m. In this way, comparison can be made considering the aspect ratio changes between both models.

B. Unducted prototype design (Gen2)

The model presented in Fig. 4 is the 1/20 prototype of the 2.5 MW-rated machines planned to be deployed during the FloWatt project. This model will be named as Gen2 in the next parts. The machine is composed of two vertical axis rotor columns, also made of two levels of rotors with a 60° phase difference between them. The model is h_{m2}= 1.010 m high, for a width with rotors of W_{m2} = 1.370 m. The rotors are : h_{r2} = 0.315m and R_{m2} = 0.235 m respectively for the height and the radius. The distance between the bottom plate and the top plate holding the rotor columns determines the turbine height : H_{m2} = 0.83 m. As in Gen1 case, a 6-component load cell of 150 daN is fixed between the turbine and the base, and a 2000 daN capacity load cell is placed below the structure. The base is composed of three lested arms, fixed to the anchor base. The arm going upstream is placed along the flow axis at flood tide. Fig. 4 presents a front view of the model.
The reference area used is composed of the green surface on the Fig.4 that is defined as the capture area $H_{m2} \times W_{m2}$, added to the area bounded by the orange outline (front surface of the base). The length between both rotor columns is L_2 = 0.76 m.

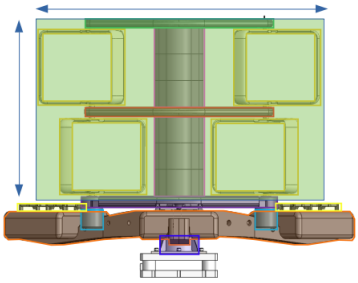

Fig. 4. Illustration (front view) of the Gen2 model. The green area and the front surface area of the base represent the total area used to normalize the hydrodynamic coefficients.

For this study, the model is not motorized. Rotors can be attached or removed, but they cannot rotate.

C. Test campaigns

The two models (Gen1 and Gen2) are tested in the wave and current circulating tank of IFREMER situated in Boulogne-sur-Mer (France). The test section is 20 m long × 4 m wide × 2 m deep (see Fig. 7). The incoming flow $(U_\infty, V_\infty, W_\infty)$ is assumed to be constant and steady, with the imposed velocity : U_∞= [0.8;1.8] m/s and $V_\infty = W_\infty = 0$ m/s. The three instantaneous velocity components are denoted (U, V, W) along the (x, y, z) directions respectively, with x the main flow direction. The model is placed at the centre of the tank, with the x-origin set at the centre of the structure (to the load cells x-position), z = 0 corresponds to the tank floor. The model is centred in the span-wise direction of the tank, with the span-wise origin (y=0) set to the centre of the model, so of the flume tank. Thanks to a grid combined with a honeycomb placed at the inlet of the working section, a low turbulence intensity $I_\infty = 1.5\%$ is reached [7] and the boundary layer height, calculated as follows $\delta_{95} = 0.95 \times U_\infty$, is equal to $\delta_{95} \approx 0.25$ m. The 3-component Laser Doppler Velocimeter (3C-LDV) measures the three velocity-components (U,V,W) at the upstream of the machine and at the centre of the turbine capture area height, more precisely at the position (x,y,z) = $(-6H_{m1}$, 0, 0.505) m for Gen1 and (x,y,z) = $(-4.3H_{m2}$, 0, 0.650) m for Gen2. At this distance upstream from the machine, the flow is not disturbed by the induction and blockage effects, and thus can be considered as a reference far upstream time average velocity named U_0. The average velocity profiles obtained in this tank configuration are shown in Fig. 5.

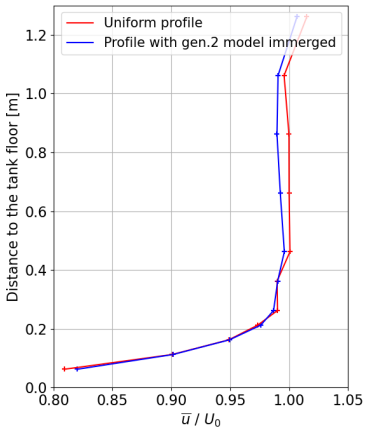

Fig. 5. Mean normalized streamwise velocity measured with 3C-LDV at the turbine position (without turbine), with z = 0 m to the tank floor. The average reference velocity U_0 is taken from flow velocity measurement at the reference position of the 3C-LDV for Gen2 configuration. Profiles are shown to be pretty similar, highlighting the fact that the flow is little disturbed by the machine with rotors at still.

Current only cases are carried out for an acquisition duration of 120s; the preliminary tests showed that values are fully converged for this duration, as the stationary state is operating before starting the test.
Two main configurations of the models are tested in order to study two flow directions (Fig. 6). Indeed, to represent ideal flood and ebb tides which are directions opposed by 180°, the turbine and the base are turned over in the tank.

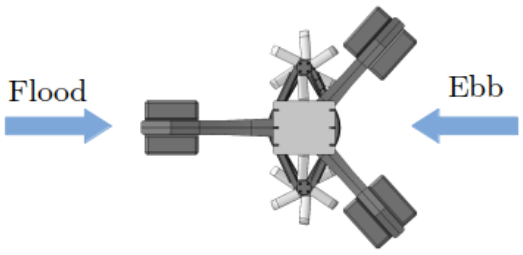

Fig. 6. Schematic view of the top of the Gen2 model with the flood and ebb tides configurations, with the turbine and the base.

To compare the wave-current interaction effects on both generations of machines, a wave-maker and a damping beach are used in order to generate waves

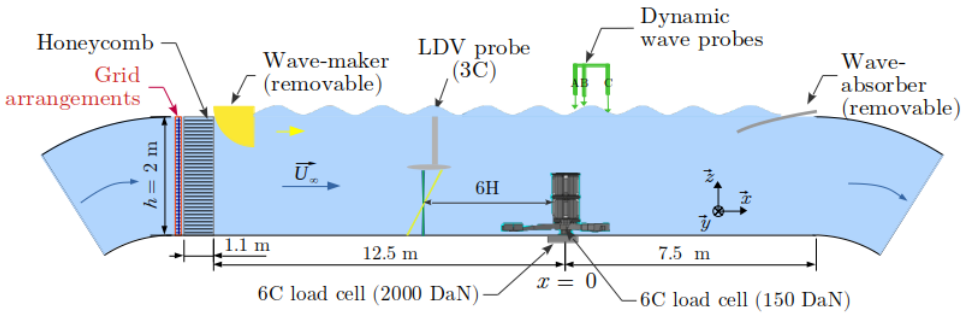

Fig. 7. Sketch of the flow configuration showing the model and the waves gauges locations, the LDV laser position and the wave-maker at the entry of the working section. Following this configuration, current flows from left to right, just like the waves.

following the current (with the configuration presented on Fig. 7), or waves opposing the current if the wave-maker is placed at the outlet of the working section (between these two configurations, the wave-maker and the damping beach positions are reversed). The damping beach (or wave-absorber) is made of a metallic porous panel (8% porosity) and is set to reduce wave reflection on the outlet wall of the working section. Wave cases generated for this study are summarized in the sections IV-A and IV-B. Five regular wave cases and one JONSWAP wave case (a type of irregular wave spectrum) are considered.

A combination of four wave gauges, three resistive wave probes and one KENEK servo-type wave probe (a dynamic probe), is used to measure the surface elevation in the flume tank. One of the resistive and the dynamic wave probes are set on the top of the machine (noted A in Fig. 7). Two other resistive probes are set to the position B and C on the scheme, with AB = 0.52 m and BC = 0.70 m. The signals from the 3C-LDV, the wave gauges and the load cells are acquired simultaneously during 200 seconds in order to reach time convergence.

III. Comparison of the flow effect for various models configurations

The effects of the sea-states conditions on the machines are first analysed in a current-stationary case and various configurations of the machines. The objective is the structural comparison between both generations using drag force and tilting moment measurements. Tests are first carried out for the basic configuration of the machines without rotors, then the results are compared with rotors at still and for different yaw angle values.

A. Structures without rotors

A first evaluation of the structure design is carried out through a comparison of the loading perceived by each element of the model. It makes it possible to study the behaviour of each element independently or not (turbine only/base/turbine+base) and to put in evidence the main structural differences between both structures. Loads and moments measured with the load cells are first compared, and then used to calculate dimensionless coefficients taking into account the designs and the test conditions.

1) Structural loading: Parameters measured by the two load cells are acquired for different current velocities and models configurations. Fig.8 presents the values obtained in the flood configuration, for many current velocities. On one hand, loads F_x applied to the turbines only (from the upper graphs) are shown to be globally higher for Gen1 than for Gen2, with an average difference of 30% in the same experimental conditions. On the other hand, the tilting moment M_y presents greater values for the case of the new design with the turbine alone, with an increase from Gen1 to Gen2 by 40% of the M_y values. Moreover, F_x and M_y data acquired with Gen2 are more scattered around the mean value than for the Gen1 measurements, which underlines the sensitivity of the new generation of turbine to toppling. This increase in tilting moment for Gen2 turbine can be explained by the height difference, Gen2 turbine being 20% higher than Gen1 turbine. Maximum and minimum values are also about 20% higher for Gen2 than in Gen1 cases. However, these variations are partly compensated when studying the turbine+base configuration. The importance of the gravity base for the structure support is then pointed out by the equivalence of the global measurements observed for the whole machine (the two lower graphs in Fig. 8). Indeed, loads and moments measured by the load cell situated below the whole structure are very similar for the current velocities tested, with less than 10% difference in drag force F_x for the same configurations. Both models thus tend to the same equilibrium regarding the responses to loading, even if some deviations remain. This is especially true for Gen2 M_y measurements which remain higher and more dispersed in extreme values, but average difference is still reduced to less than 16%. The same tendencies are noticeable for the ebb tide configuration, with higher F_x values for Gen1 and M_y for Gen2 in turbine only case, but this gap decreases when the base and the turbine are studied together.

2) Dimensionless coefficients C_x and C_{My} comparison: As the design has evolved between the two generations, it is important to take into account the specific geometry of each model. Coefficients defined

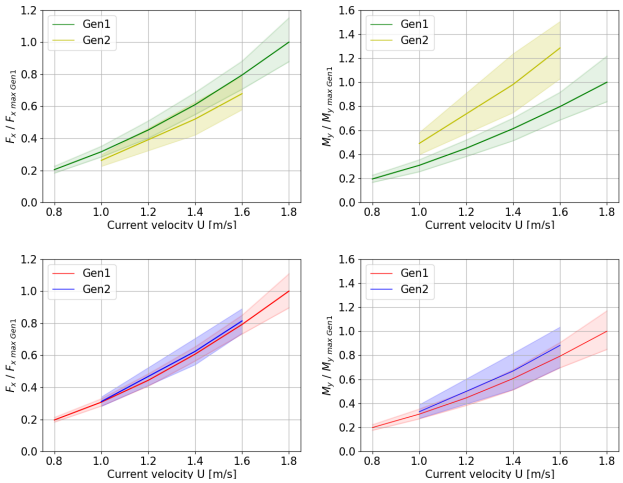

Fig. 8. Representation of average loads F_x and moments M_y (continuous lines) and their min/max values (transparent areas) measured for both machines without rotors at flood tide. On the left : measures of the loads F_x. On the right : measures of the moments M_y. Upper graphs : Values acquired for the turbine only case. Lower graphs : Values obtained with the entire structure (turbine + base). Same tendencies are observed with the ebb tide configuration.

in II are thus calculated using the acquired data, specifically for both configurations and their own reference surface/length. Thus proceeding to the non-dimensionalization regarding loading, surface and current velocity, Gen1 cases coefficients are found similar just like Gen2 cases. This is justified by the tendency in the Fig. 9.

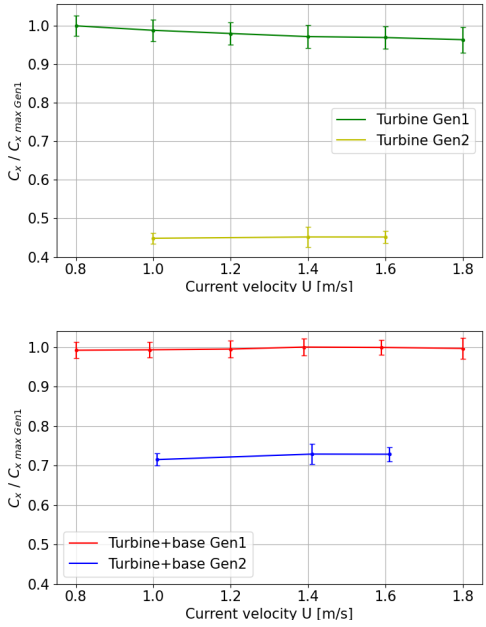

Fig. 9. Representation of dimensionless drag coefficients $C_x/C_{x\ max\ Gen1}$ (continuous lines) and their standard deviations (errorbars) calculated for both models without rotors at flood tide, with $C_{x\ max\ Gen1}$ the maximum coefficient value obtained for these Gen1 case. The upper graph represents the coefficients calculated from data acquired for the turbine only. The lower graph illustrates the difference between coefficients for the turbine+base configuration. M_y are not shown but their tendencies are described in III-A2.

Without rotors, it is observed that loads and moments-related coefficients are higher in Gen1 compared to the new design. As illustrated in Fig.9 (upper graph), a difference of almost 50% of the coefficients is visible between the turbine only cases for drag coefficients, and tilting moment coefficients are also 30% higher for Gen1 compared to Gen2. This gap is a little reduced in the turbine+base cases (lower graph), with Gen1 coefficients about 25% higher than Gen2 ones for the drag, and 35% higher for the tilting moment. By its design, Gen1 structure appears to be more constrained by the flow conditions as the efforts are less distributed on the structure. Refering to the Fig. 8, a closeness between drag and tilting moment raw values for both models can be seen, but the geometrical modification induces an alteration in the way prototypes perceive it. Regarding the dependency to reference area and length, the influence of the design is clearly exposed through this interpretation of loading.

B. Prototypes with rotors at still

In the same way, models designs influence is investigated for the same configuration as before to which is added the fixed rotors. In addition to the design variations, the structural response will also be altered by the rotors shape. Values of the coefficients are given in Table I. The only difference between both ranges of tests is the velocity current change. As we are interested in dimensionless coefficients, these variations are taken into account in the coefficients definitions and do not impact our analysis procedure, as proven by the study of the Fig. 9. As we do not modify

TABLE I
VALUES OF C_x AND C_{My} AND THEIR STANDARD DEVIATIONS OBTAINED WITH THE ROTORS AT STILL AND IN PRESENCE OF CURRENT.

Elements studied	$\lvert C_x \rvert$	$\sigma(C_x)$	$\lvert C_{My} \rvert$	$\sigma(C_{My})$
Flood tide				
Gen1 turbine+base	0.554	0.010	0.350	0.010
Gen2 turbine+base	0.478	0.009	0.304	0.009
Gen1 turbine	0.435	0.010	0.335	0.009
Gen2 turbine	0.372	0.007	0.289	0.007
Ebb tide				
Gen1 turbine+base	0.567	0.008	0.380	0.009
Gen2 turbine+base	0.435	0.007	0.311	0.008
Gen1 turbine	0.426	0.008	0.333	0.008
Gen2 turbine	0.382	0.007	0.293	0.007

the way of calculating the coefficients, particularly by keeping the same reference areas, both C_x and C_{My} coefficients increase compared to the ones found in III-A2. Indeed, the increase in loads and moments is expected because the load application area increases for the same reference surface (to the green surface is added rotors at still). Between the two generations, with rotors at still, the C_x coefficient is lower of about 15% for Gen2 compared to Gen1 values. Comparing to III-A2, the presence of the rotors seems to lessen the gap of C_x values even if Gen1 values remain higher. Larger coefficients are also observed in Table I for the C_{My} coefficients compared to cases without rotors. However, just like the C_x tendencies with the rotors

fixed, the C_{My} variation from Gen1 to Gen2 is approximately 15% while it was 35% without rotors. Rotors shape and dimensions generate a tilting moment due to the grip they have on the flow. Standard deviation of both coefficients remains the same in both Gen1 and Gen2 cases for the same configuration. Addition of rotors to Gen2 structure has a great effect on the perceived load.

C. Effects of the yaw angle change

As an origin of performance issue, determining a great positioning of the machine is pretty important. A misalignement from the established flow direction can impact performance and results in uncertainties [8]. To go further in the analysis of current-induced loading, various yaw angles are tested for both models to see how the misalignement affects the models designs.

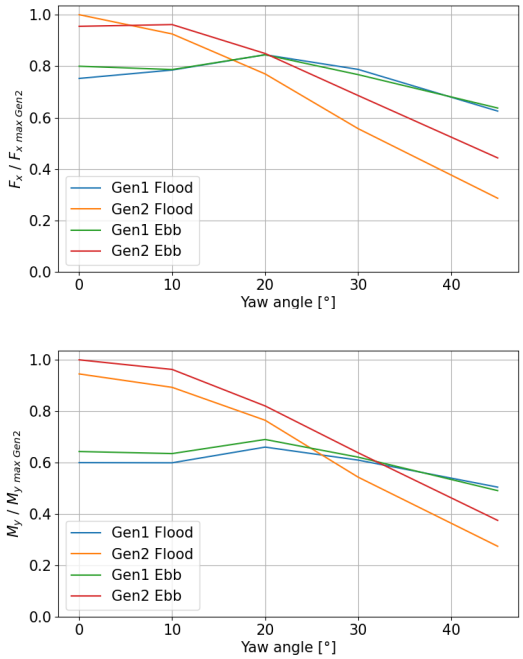

Fig. 10. Representation of the normalized drag force F_x and the tilting moment M_y expressed as a function of the yaw angle imposed to the models. Loadings have been normalized by the highest values obtained $F_{x\ max}$ and $M_{y\ max}$. Tendencies between both graphs are found similar.

To do so, drag force and tilting moment measured values are compared for different yaw angles of the models in relation to the flow direction. This is possible thanks to the rotating bottom of the flume tank on which models are disposed. Tendencies are here the points of divergence between the two generations of machines.
First, looking to the graphs in Fig.10, the same trend in curves evolution can be seen for F_x and M_y. For both configurations Flood/Ebb tides, Gen1 values tend to a maximum around 20°, and then curves decline. On both graphs, Gen1 starting and ending values are pretty identical (between 0° and 45°). However, for the Gen2 cases, as the angle increases from 0 to 45°, the values of both quantities decrease. Another impact of the design changes is put in evidence by these results : the front surfaces to the flow evolve in a different way, as Gen1 perceives more loads being applied to it than to Gen2. A main design characteristic of the ducted prototype (Gen1) is thus highlighted, compared to the unducted one (Gen2) which only presents a decrease of the loads when the yaw angle increases.

Main differences induced by the design of each model are shown, considering loading variations between both prototypes and their own geometry. A next step will be the characterisation of the models under other constraints, mainly due to the sea states.

IV. Waves impact on the machines

To go further in the characterisation of the machines response, the effects of surface waves on the models are investigated in this section. Different amplitudes and frequencies of waves are tested to evaluate their influence. Impacts of waves following the current are first investigated. Then, the effects of waves against the current cases are examined.
The results presented here are related to the data acquired for Gen2. The comparison with the results of Gen1 is made in section IV-C. All measurements in this section are carried out for a current velocity U_0 = 0.8 m/s.

A. Waves following the current

To characterize the effects of waves following the current, three cases of various amplitudes of waves with the same frequency and three cases with different frequencies but with a similar amplitude are used. Wave parameters and names are given in Table II. A JONSWAP case (irregular wave case) is also tested, with a peak period T_s = 1.67 s and a significant wave height H_s = 105 mm. Results presented in this section were obtained for the model in flood tide configuration, so that the model faces the current.

TABLE II
Waves following the current parameters : name, wave frequency, mean wave amplitude (Low/Medium/High) and wavelength.

Name	f_h [Hz]	$\overline{A}$ [mm]	λ [m]
$f075L$	0.750	20	3.7
$f075M$	0.750	75	4.3
$f075H$	0.750	110	3.7
$f050M$	0.500	65	6.2
$f060M$	0.595	70	5.6

First, the Fourier transform of the F_x signals acquired by the load cell situated below the structure are done in order to look for wave-related components. As shown in the Fig. 11, main components of the signals are found to be at the wave frequencies. It can be assumed that waves influence the loading applied to the models.

In addition to the signatures at the wave frequencies, the sub-harmonic of the $f050M$ is visible at 1.0 Hz, on the contrary of the other wave case sub-harmonics which are embedded in the high frequency noise. PSD illustrates the dissipation of the other sub-harmonics,

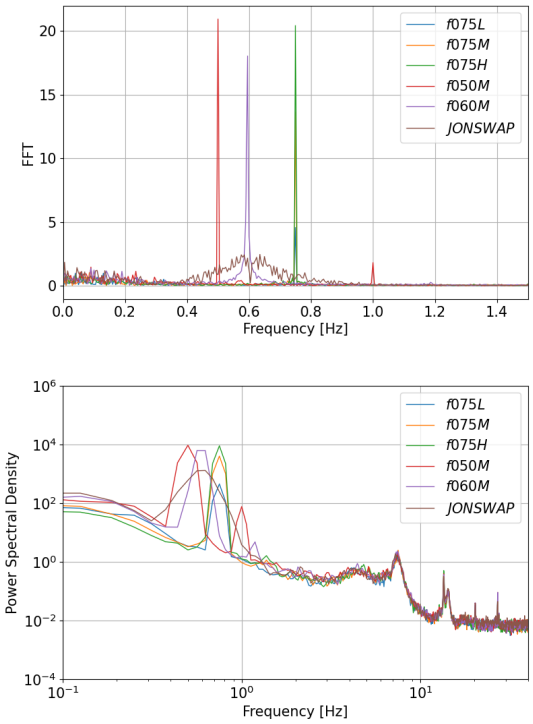

Fig. 11. Upper : Fourier transforms of the F_x signals from the cases of waves following the current at flood tide. Lower : Power Spectral Density of the F_x signals from the cases of waves following the current at flood tide. Wave signatures are present around wave characteristic frequency (main peaks).

with only the $f050M$ one truly relevant compared to the others. At the $f050M$ wave frequency, a specific mode of the model must be excited in the tank, and could thus explain this energetic peak. This particular element can be a point of interest for future works with wave-current-Gen2 model interaction. In higher frequency range, signals have comparable evolution with the same tendencies.
Then, average loads and their standard deviations are measured and represented in the Fig. 12. To the wave cases is compared a one named 'f075Msc', with the same wave characteristics as 'f075M' but without current. By first comparing these two cases, the current appears to be the main contributor to the applied loads. Indeed, the drag force in the presence of waves without current represents only 13% of the average drag observed for the waves+current cases. JONSWAP case also seems to have a similar effect on loads that regular wave case with a wave period close to the peak period associated to the JONSWAP one. Now comparing the effects of waves parameters, the loads increase when the amplitude increases for a same frequency. In the Fig. 12, there is a rise of average loads by 5% from $f075L$ to $f075H$. Moreover, for the lower wave frequencies, loads are found to be higher. From $f075M$ to $f050M$ (cases with different frequencies but the same amplitude), drag force increases by 5%. A cause of this difference is the wave behaviour in the water column regarding its parameters. Lower wave frequencies tend to penetrate better the water column, and so have a greater impact on the model.

Same kind of average tilting moment variations happens but with a less pronounced difference, as values differences between wave cases are not exceeding 4%. Though the same standard deviations ratios are noticeable as for F_x.

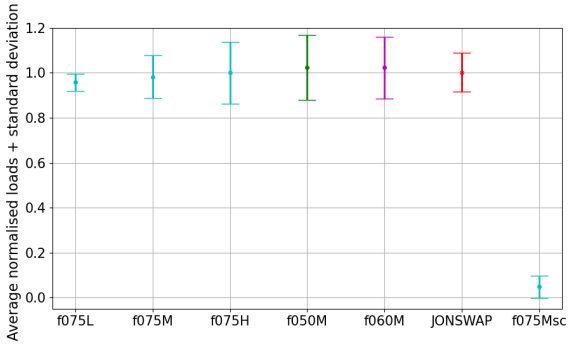

Fig. 12. Average normalized loads and their standard deviations measured for the cases of waves following the current at flood tide. 'sc' case corresponds to a control case without current and the same wave conditions than 'f075M'. Average loads are normalized by the one obtained for the $f075H$ case.

For waves following the current, waves have been shown to induce load strengthening on the machine, as it penetrates the water column to a greater or lesser extent depending on wave frequency and amplitude. In these cases, the loading is maximized for the $f050M$ case, with the lowest frequency and the medium amplitude. On may wonder about the results that would be obtained for waves at the same frequency but with a higher amplitude, which could have a great impact on the loading seen by the model.

B. *Waves opposing the current*

After seeing the loads increase linked to the wave cases and its dependency to wave parameters for waves following the current, evolution of waves effects for waves opposing the current can be considered. To do so, as in the previous section, three amplitudes and frequencies are used to characterize the models response to wave action at the ebb tide configuration. Doing so, the waves remain in the same configuration regarding the model. Wave opposing the current cases are presented in Table III.

TABLE III
WAVES OPPOSING THE CURRENT PARAMETERS : NAME, WAVE FREQUENCY, MEAN WAVE AMPLITUDE (LOW/MEDIUM/HIGH) AND WAVELENGTH.

Name	f_h **[Hz]**	$\overline{A}$ **[mm]**	λ **[m]**
$f040L$	0.405	30	5.0
$f040M$	0.405	75	4.9
$f040H$	0.405	100	4.9
$f030L$	0.295	30	/
$f050L$	0.500	30	3.3

A JONSWAP wave case is also studied, with a peak period about T_s = 2.5 s and a significant wave height H_s = 100 mm. A Fourier analysis is done for the F_x signals using Fourier transform and Power Spectral

Density in the Fig. 13, highlighting main frequency components at the wave frequencies. Tendencies of the PSD remain the same between the different cases, which makes waves and current the two major parameters conditioning the loading. Sub-harmonics of $f040H$ are pretty visible, a high wave amplitude increasing its effects on the loads.

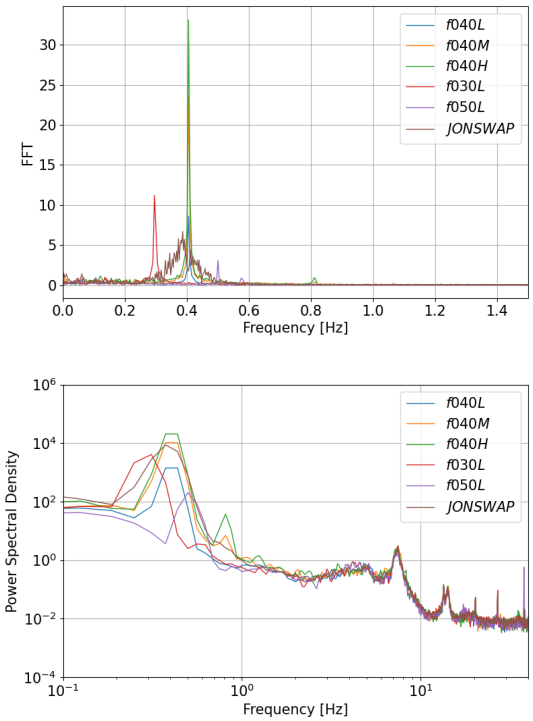

Fig. 13. Upper : Fourier transforms of the F_x signals from the cases of waves opposing the current at ebb tide. Lower : Power Spectral Density of the F_x signals from the cases of waves opposing the current at ebb tide. "...sc" = control case without current. Wave signatures are present around wave characteristic frequency (main peaks).

Load values and their standard deviations are presented in Fig. 14. Drag force without current represents 14% of the load measured for the same wave case with current, pointing out the importance of studying the wave-current interaction to consider the coupling between the two main contributors to model loading.

Average loads are globally similar with less than 8% difference between two cases loading values. Nevertheless, wave cases with the highest amplitudes present higher values than the lower ones as shown by the increase of loading for the $f040\_$ cases when wave amplitude increases. Standard deviations are also scattered, representing from 3% of the average load for low amplitude cases to 20% for the highest amplitude. Waves opposing the current are then an impacting factor concerning the load application to the model. By studying tilting moment values, same tendencies are observed but are more pronounced, with higher differences between lower wave amplitude cases and the highest one ($f040H$) of the order of 10%.

As observed in previous studies [9], the lower the frequency and the higher the amplitude, the more the waves tend to penetrate the water column. From the

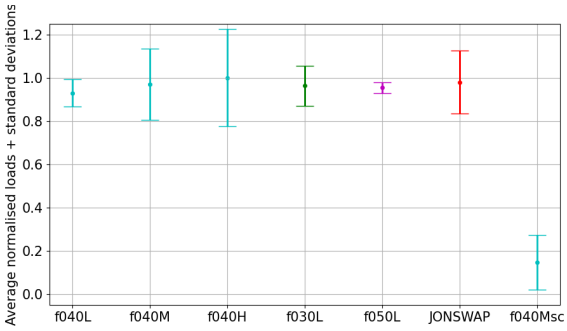

Fig. 14. Average loads and their standard deviation [N] measured for the waves opposing the current cases at ebb tide. 'sc' case corresponds to a control case without waves.

results, waves opposing the current seem to have a more pronounced impact than waves following the current, their effects and variations are then better perceived. In light of these results, as the wave-current interaction takes part in a non-negligible way on the loads, attention should be paid to it in future studies on current-waves-Gen2 interaction.

Wave-current interaction modifies the conditions that the machine must undergo. The most impacting case here is the $f040H$ one, with a low frequency and and the highest amplitude. Waves presence thus participates to a loading reinforcement, depending on wave parameters. A thorough study of the model behaviour under this complex environment is then necessary to take the most of model performance.

C. *Waves effects on both generations of machines*

The loads applied to the Gen2 model are affected by waves, both in the case of waves following and opposing the current. Main differences seem to lie in the ability of waves to penetrate the water column. Waves with higher amplitude and lower frequency seem to have a more significant impact. In order to see how the design affects loading variations, Gen2 wave cases are compared to the Gen1 ones with the same wave configurations and parameters as in the last subsections.

As it can be observed on the graphs in Fig. 15, drag force and tilting moment values are respectively 20% and almost 40% higher in Gen2 case compared to Gen1 for waves following the current. A similar ratio is observed in Fig. 10 for the 0° position, but an increase of a few percent happens for some wave cases (especially on M_y for high amplitude waves) as the Gen2 is taller and then more sensitive to wave effects. Dimensionless coefficients support the tendency previously observed for cases without waves, as Gen2 C_x and C_{My} are 10 to 20% lower than Gen1 ones (Table IV). Indeed, these ratios are equivalent to those that can be found in I. The same applies to waves opposing the current, with higher loading on Gen2.

In view of the results, wave cases globally act in the same way on both machines, with the conservation of the Gen1/Gen2 ratio values. Parts IV-A and IV-B

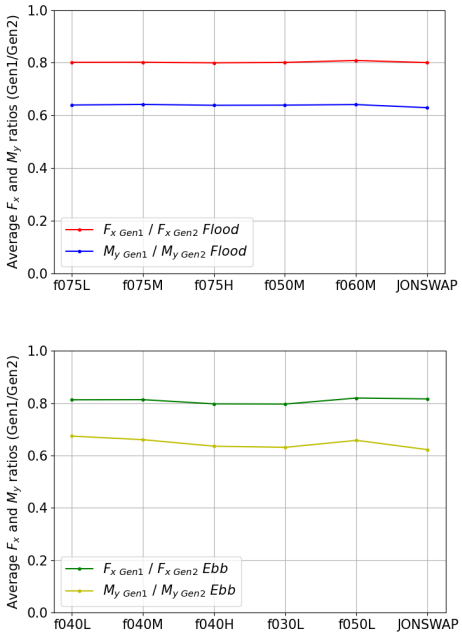

Fig. 15. Average F_x and M_y ratios defined as Gen1/Gen2 values. Upper graph : ratios calculated for the waves following the current cases (Flood). Lower graph : ratios calculated for the waves opposing the current cases (Ebb).

TABLE IV
VALUES OF AVERAGE C_x AND C_{My} OBTAINED WITH THE ROTORS AT STILL, IN PRESENCE OF CURRENT AND WITH WAVES FOLLOWING THE CURRENT.

Cases	Gen1 $\lvert C_x \rvert$	Gen2 $\lvert C_x \rvert$	Gen1 $\lvert C_{My} \rvert$	Gen2 $\lvert C_{My} \rvert$
$f075L$	0.520	0.419	0.327	0.274
$f075M$	0.524	0.413	0.328	0.268
$f075H$	0.527	0.411	0.327	0.265
$f050M$	0.526	0.435	0.325	0.280
$f060M$	0.529	0.435	0.323	0.277

showed that an increase in loading happened under waves conditions, so Gen1 model is also subjected to equivalent increased loading. Even so, for some cases, wave effect seems stronger on Gen2 in increasing the differences between the models values. This may be linked to its height, which makes it more affected by the waves. However, its design remains more optimal than Gen1 geometry as the dimensionless coefficients are found to remain lower.

V. CONCLUSION

In this paper, two twin vertical axis tidal turbine designs are investigated through load measurements. Drag force and tilting moment are measured for the different elements of the machine (turbine+base). First, the importance of each element is exposed studying the models structural response to loading without rotors. Both turbines having two different geometries, the addition of bases makes both models similar in the load undergone. However, the load distribution is not the same as the capture areas differ, which is perceptible through the hydrodynamic coefficients used. Gen2 presents lower coefficients, with a decrease of about 15% from Gen1 to Gen2 values without the rotors. With rotors at still, this difference still exist but is lessened as the perceived loads increase for Gen2. The geometry distinction is also pointed out by the models response to yaw angle change, as loading tendencies are diverging.

To go further in the characterisation of the model under flow conditions, the effects of the waves on the loading is highlighted through a Fourier analysis of the loads measurements. Then a first approach of how the waves amplitude and frequency modify it is carried out. It first appears that the lower the frequency and the higher the amplitude, the higher the loads perceived by the models. Complementary tests will provide a better definition of the phenomenon.

Through these elements, influences of the geometry and design of each model have been compared. Gen2 design seems better optimized as it presents a better loading distribution and response to the imposed flow conditions. Even though the loads remain globally higher in magnitude, design is better suited to deal with it, revealed through the study of the dimensionless coefficients.

An in-depth investigation about the Gen2 behaviour is motivated to the light of these results. A next step will be a broader understanding and characterisation of its operating state. The studies of Gen2 wake and performance with rotors operating will thus provide more information. As global tendencies remain pretty equivalent between the two generations, the studies carried out for Gen1 will help anticipate and optimize testing of Gen2, further justifying the design choices.

REFERENCES

[1] N. Guillou, S. Neill, and P. Robins, "Characterising the tidal stream power resource around france using a high-resolution harmonic database," *Renewable Energy*, vol. 123, 02 2018.
[2] M. Moreau, G. Germain, G. Maurice, A. Richard, and R. Coquet, "Hydroquest: Feedback from paimpol-brhat and validation of the design method," 09 2021.
[3] M. Grondeau, G. Sylvain, P. Mercier, and E. Poizot, "Wake of a ducted vertical axis tidal turbine in turbulent flows, lbm actuator-line approach," *Energies*, vol. 12, p. 4273, 11 2019.
[4] N. Guillaud, G. Balarac, E. Goncalves, and J. Zanette, "Large eddy simulations on vertical axis hydrokinetic turbines - power coefficient analysis for various solidities," *Renewable Energy*, vol. 147, 08 2019.
[5] M. Moreau, C. Derveaux, G. Maurice, J.-V. Facq, and G. Germain, "Experimental study of two opposed flow directions effect on a ducted twin vertical axis tidal turbine," *Trends in Renewable Energies Offshore*, pp. 161–167, 2022.
[6] G. G. M. G. Bloch Noam, Moreau Martin, "Experimental study of bathymetry variation effects on a cross-flow water turbine," FRANCE, 2022. [Online]. Available: https://archimer.ifremer.fr/doc/00808/91953/
[7] D. P. G. B. Ikhennicheu Maria, Germain Gregory, "Experimental study of coherent flow structures past a wall-mounted square cylinder," FRANCE, pp. 137–146, 2019.
[8] L. Evans, I. Ashton, and B. G. Sellar, "Impact on energy yield of varying turbine designs under conditions of misalignment to the current flow," *Energies*, vol. 16, no. 9, 2023. [Online]. Available: https://www.mdpi.com/1996-1073/16/9/3923
[9] Y. Saouli, M. Magnier, G. Germain, B. Gaurier, and P. Druault, "Experimental characterisation of the waves propagating against current effects on the wake of a wide bathymetric obstacle," 11 2022.